Bearing Fault Diagnosis Method for Single-Channel Vibration Signal Using 1D and 2D Feature Fusion

BIN-BIN QIU[1,2], SI-QI LIU[1], WEI-DONG LI[1], LI-HUI WANG[2] and XI-VINCENT WANG[2]

ABSTRACT

Conventional methods for diagnosing bearing faults typically depend on multiple sensors to monitor the operational state of equipment. However, in practical applications, space constraints often limit sensor placement, making it difficult to ensure diagnostic accuracy. This study proposes a fault diagnosis method based on the fusion of one-dimensional and two-dimensional features extracted from a single-channel vibration signal. Firstly, one-dimensional time-domain and frequency-domain features are extracted from the vibration signal. The minimum Redundancy Maximum Relevance (MRMR) method is employed to select key features that have strong correlation with fault types while minimizing redundancy. Secondly, the single-channel vibration signal is converted into a two-dimensional image using the Gramian Angular Difference Field (GADF) method, and a Convolutional Neural Network (CNN) is employed to automatically extract high-level image features. The optimized one-dimensional feature vector is then fused with the two-dimensional image feature vector to create a high-dimensional feature representation, and the Support Vector Machine (SVM) is utilized to identify fault types based on the fused feature vector. The experimental results show that the feature fusion strategy using only single-channel vibration signals significantly improves the accuracy of fault diagnosis and provides an effective and interpretable solution for industrial fault diagnosis.[1]

1 INTRODUCTION

In modern industrial manufacturing, the operational stability of critical equipment heavily relies on the reliability of bearings. Their failure may lead to unplanned downtime or even catastrophic system breakdowns, resulting in significant economic losses and safety hazards [1]. Vibration monitoring has proven effective in equipment health status, but the diagnostic process is particularly challenging for complex mechanical systems such as gearboxes. Here, multi-source interferences (e.g., gear meshing, shaft torsion, etc.) often cause bearing fault features to be obscured by strong background noise [2]. Although traditional machine learning approaches (e.g., gradient boosted decision trees, support vector machines (SVM), and random forests (RF)) have demonstrated practical value in fault diagnosis, their effectiveness remains constrained by inherent limitations in feature engineering. The quality of features directly affects model performance, and

[1]School of Mechanical Engineering, University of Shanghai for Science and Technology, Shanghai, China
[2]Department of Production Engineering, KTH Royal Institute of Technology, Stockholm, Sweden

these methods struggle to represent the complex coupling characteristics of faults [3-6].

Some researchers have explored feature optimization using the mRMR algorithm, which selects features by maximizing relevance to fault categories and minimizing redundancy. For example, Yan et al. [7] combined mRMR with multi-scale dispersion entropy and ELM to automatically select sensitive features for fault diagnosis. Ghasimi et al. [8] used mRMR with wavelet transform and a linear SVM, improving classification accuracy. These studies show the effectiveness of mRMR in extracting key fault features from vibration signals.

With the advancement of Industry 4.0, deep learning—due to its automatic feature extraction—has become a frontier in bearing fault diagnosis research. To overcome the limitations of manual feature engineering, researchers use methods like multi-modal signal transformation, spatiotemporal fusion, and attention mechanisms. For instance, Cai et al. [9] converted 1D vibration signals into 2D images with Markov transition fields and applied SE-IShufflenetV2 for fault identification. Wu et al. [10] combined multi-scale CNN, LSTM, and attention to achieve strong, noise-resistant diagnosis under variable loads. Despite reducing reliance on manual feature engineering, high-dimensional feature redundancy still limits model efficiency.

In addition to the challenges of feature extraction mentioned above, sensor placement, environmental factors, and costs further limit the practical application of fault diagnosis methods. This study proposes a feature fusion-based diagnostic method based on single-channel vibration signals, aiming to enhance fault recognition capability by integrating time-domain, frequency-domain, and image features. The specific process involves: 1) extracting time-domain/frequency-domain features and selecting key features using the mRMR algorithm; 2) converting the temporal signal into a two-dimensional image via Gramian Angular Difference Field (GADF) and extracting high-level image features using CNN; 3) fusing the two types of features and inputting them into SVM for classification. Experimental results demonstrate that the proposed method achieves a diagnostic accuracy of 99.9% under small-sample conditions (100 samples per category). Moreover, it demonstrates strong adaptability to sensor position changes. This method effectively addresses the challenge of insufficient fault feature information in small-sample scenarios and provides a new solution for intelligent maintenance of rotating machinery.

2 THEORETICAL FOUNDATIONS AND THE PROPOSED APPROACH

2.1 MINIMUM REDUDANCY MAXIMUM RELEVANT (mRMR)

The mRMR method is an efficient information-theoretic feature selection technique that simultaneously maximises the relevance to the target variable and minimises redundancy between features. This dual-objective approach efficiently selects a compact and discriminative subset of features, thus balancing diagnostic accuracy and computational efficiency in engineering applications. The goal of the mRMR method is to establish a balance between maximum relevance and minimum redundancy. The objective function of mRMR is defined in equation (1).

$$\max\left[\frac{1}{|S|}\sum_{x_i\in S} I(x_i,c)-\frac{1}{|S|^2}\sum_{x_i,x_j\in S} I(x_i,x_j)\right] \tag{1}$$

where x_i and x_j are features in the feature set S, c is the target variable. Relevance in equation (1) is defined as follows:

$$I(X,Y)=\sum_{x\in X}\sum_{y\in Y}p(x,y)\log\frac{p(x,y)}{p(x)p(y)} \tag{2}$$

where X is the feature variable, Y is the class label, $p(x,y)$ represents the joint probability distribution of X and Y, and $p(x)p(y)$ denotes the marginal probabilities of X and Y respectively.

2.2 THE PROPOSED APPROACH

To improve the accuracy and generalization ability of bearing fault diagnosis, this study proposes a fault diagnosis method based on the fusion of 1D and 2D features extracted from single-channel vibration signals. The model mainly consists of five parts: data acquisition, 1D feature extraction, 2D feature extraction, feature fusion and fault classification, as shown in Figure 1.

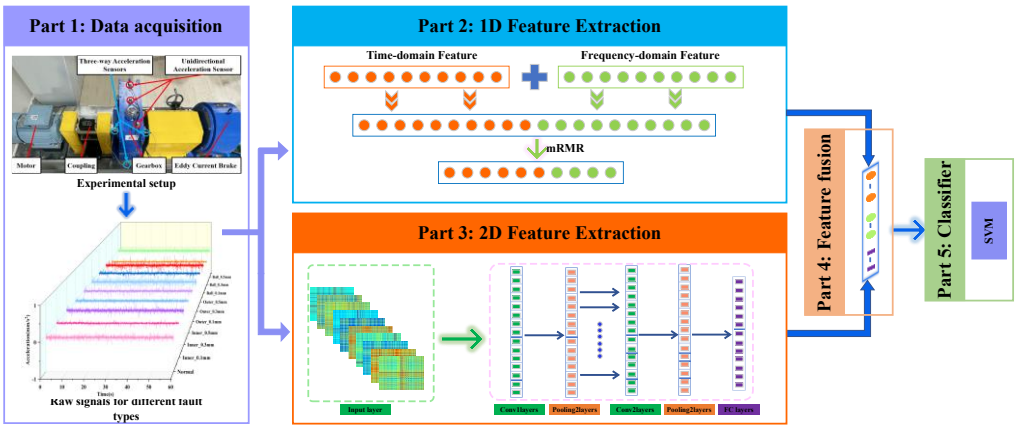

Figure 1. Proposed model framework

Part 1: Data acquisition

The vibration signals of bearings are collected through acceleration sensors, which encompass the vibration characteristics under varying loads, rotational speeds, and other operating conditions, thereby providing raw data for subsequent analysis.

Part 2: 1D feature extraction

In this part, the time-domain and frequency-domain features in Table I are extracted, and then the features are screened using the mRMR algorithm to improve the computational efficiency and accuracy of the model.

Part 3: 2D feature extraction

The raw signals are converted into 2D images using the GADF method. These transformed images are then processed through a CNN to extract deep image features, capturing complex spatial relationships within the signals.

Part 4: Feature fusion

In the feature fusion stage, the screened time-domain and frequency-domain features are fused with the 2D image features extracted by CNN, resulting in a high-dimensional feature vector.

Part 5: Fault classification

In the fault classification stage, the fused high-dimensional feature vector is fed into the SVM classifier for training and testing. By maximizing the margin between classes, the SVM effectively distinguishes different fault types, enabling accurate classification of fault conditions.

TABLE I. TIME DOMAIN FEATURES AND FREQUENCY DOMAIN FEATURES

No.	Time-domain feature (TF)	Formula	No.	Frequency-domain feature (FF)	Formula
1	Mean	$\mu = \frac{1}{N}\sum_{N}^{i=1} x_i$	1	Dominant Frequency	$f_d = \arg\max \lvert X(f) \rvert$
2	Variance	$\sigma^2 = \frac{1}{N}\sum_{N}^{i=1}(x_i - \mu)^2$	2	Spectral Energy	$E = \sum \lvert X(f) \rvert^2$
3	Standard Deviation	$\sigma = \sqrt{\sigma^2}$	3	Mean Frequency	$f_{\text{mean}} = \frac{\sum f \cdot \lvert X(f) \rvert}{\sum \lvert X(f) \rvert}$
4	Peak	$\max(\lvert x_i \rvert)$	4	Standard Deviation of Frequency	$\sqrt{\sum (f - f_{\text{mean}})^2 \cdot \lvert X(f) \rvert}$
5	Peak Factor	$\frac{\max(\lvert x_i \rvert)}{\text{RMS}}$	5	Frequency Peak Value	$\max(\lvert X(f) \rvert)$
6	Skewness	$\frac{1}{N}\sum_{N}^{i=1}\left(\frac{x_i - \mu}{\sigma}\right)^3$	6	Bandwidth	$\sqrt{\frac{\sum (f - f_c)^2 \cdot \lvert X(f) \rvert^2}{\sum \lvert X(f) \rvert^2}}$
7	Kurtosis	$\frac{1}{N}\sum_{N}^{i=1}\left(\frac{x_i - \mu}{\sigma}\right)^4$	7	Total Energy	$\int \lvert X(f) \rvert^2 \, df$
8	Margin Factor	$\frac{\max(\lvert x_i \rvert)}{\left(\frac{1}{N}\sum_{N}^{i=1} \lvert x_i \rvert\right)^2}$	8	Spectral Entropy	$-\sum_f p(f)\log(p(f))$
9	Impulse Factor	$\frac{\max(\lvert x_i \rvert)}{\frac{1}{N}\sum_{N}^{i=1} \lvert x_i \rvert}$	9	Spectral Skewness	$\frac{1}{N}\sum_{N}^{i=1}\left(\frac{X(f) - \mu}{\sigma}\right)^3$
10	Shape Factor	$\frac{\text{RMS}}{\frac{1}{N}\sum_{N}^{i=1} \lvert x_i \rvert}$	10	Spectral Kurtosis	$\frac{1}{N}\sum_{N}^{i=1}\left(\frac{X(f) - \mu}{\sigma}\right)^4$

3 EXPERIMENTS AND RESULTS

3.1 EXPERIMENTAL SETUP

In this study, a bearing fault diagnosis experimental platform (as shown in Figure 2) was used for the validation of the proposed method. The experimental setup primarily consists of a motor, coupling, gearbox, eddy current brake, electrical cabinet, and acceleration sensors. The motor runs at 1710 r/min. The eddy current brake applies load currents of 0.3A and 0.5A to simulate different operating conditions. Inside the gearbox, bearings with various fault types are installed, including normal bearing, inner ring faults (0.1mm, 0.3mm, 0.5mm), outer ring faults (0.1mm, 0.3mm, 0.5mm), and ball faults (0.1mm, 0.3mm, 0.5mm), ensuring the diversity and comprehensiveness of the dataset. Vibration signals are collected by acceleration sensors at 10 kHz with a sampling length of 1024 points, yielding 100 samples per fault type and load condition.

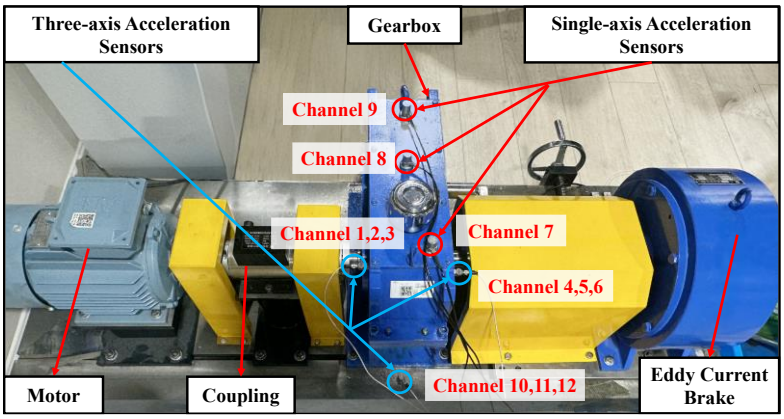

Figure 2. Faulty bearing test bench

The experimental dataset includes four parts: Dataset A (0A load, no-load state), Dataset B (0.3A load, light load), Dataset C (0.5A load, heavy load) and Dataset D (a mixture of Datasets A, B, and C). Each is split 80% for training and 20% for testing to ensure data representativeness and effective model learning and generalization across different load conditions.

3.2 DISCUSSION ON SENSOR PLACEMENT

In practical applications, the placement of sensors directly affects the effectiveness of fault diagnosis. To verify that single-channel vibration signals can achieve effective fault diagnosis, this study deployed sensors at various positions on the experimental platform to collect corresponding vibration signals. A total of six acceleration sensors were used in the experiment, including three single-axis acceleration sensors and three three-axial acceleration sensors, yielding a total of 12 data channels. These sensors were installed at multiple key measurement points on the experimental platform to capture vibration data from different locations. The fault diagnosis analysis conducted on different channel data is shown in Figure 3.

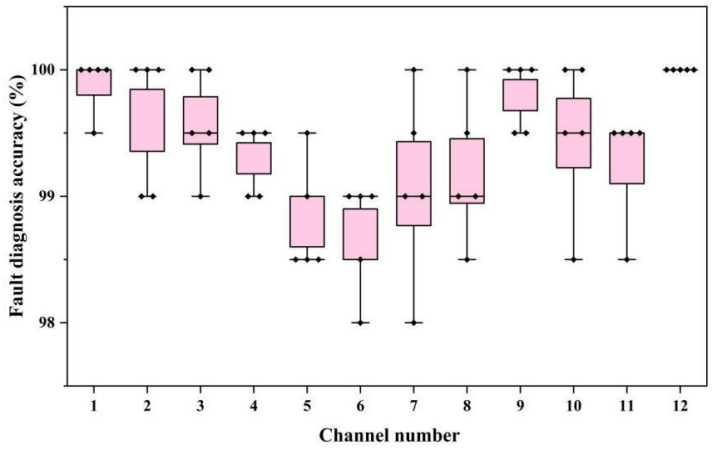

Figure 3. Diagnostic results of different sensor positions

As shown in Figure 3, the proposed method achieves effective fault diagnosis with high accuracy regardless of sensor placement location on the gearbox. This simple sensor solution significantly reduces hardware cost and system complexity by fusing multi-dimensional features of single-channel vibration signals while

guaranteeing fault diagnosis accuracy. Compared with multi-channel data-dependent solutions, the proposed method effectively avoids the need for complex deployment configurations and large-scale data collection, thereby providing a more efficient solution for bearing fault diagnosis.

3.3 APPROACH VALIDATION UNDER VARIABLE OPERATING CONDITIONS

The ability to generalise the model is crucial in the task of bearing fault diagnosis. Therefore, this study conducts cross-condition validation by constructing individual load datasets and a mixed-load dataset. The experimental results are presented in Table II.

TABLE II. Diagnosis results for load input currents of (A) 0.0A, (B) 0.3A, (C) 0.5A, (D)mixture

Datasets	Fault diagnosis accuracy					
	First run	Second run	Third run	Fourth run	Fifth run	Average
A	99.5	100	100	100	100	**99.9**
B	99.5	100	100	100	100	**99.9**
C	99.5	99	99.5	99	99.5	**99.3**
D	99.17	100	99.17	100	99.17	**99.5**

As indicated in Table II, the model maintains near-perfect accuracy (approaching 100%) under both 0A and 0.3A load conditions, demonstrating excellent performance. When the load current increases to 0.5A, although the accuracy slightly decreases, it still remains above 99%, confirming the strong robustness of the model. Even when tested on the mixed-load dataset D, the diagnostic accuracy also stays above 99%, indicating good environmental adaptability and generalization capability. These results indicate that the model has reliable fault identification capability under different load scenarios, meeting the requirements of real-world engineering applications. It is particularly well-suited for deployment in industrial diagnostic systems that involve multi-condition integration.

3.4 NOISE RESISTANCE PERFORMANCE ANALYSIS

To systematically assess the anti-interference capability of the diagnostic model, controlled noise of varying intensities is superimposed onto the original vibration data and different noise environments are quantitatively simulated through adjustments of the signal-to-noise ratio (SNR). The SNR is computed based on a logarithmic expression of the energy ratio, formally defined as:

$$SNR(dB) = 10\log_{10}(\frac{P_{signal}}{P_{noise}}) \tag{3}$$

where P_{signal} is the signal power, and P_{noise} is the noise power. This study systematically evaluates the noise immunity performance of the fault diagnosis model across scenarios spanning from extreme noise (-10dB) to typical industrial noise (10dB). It focuses on its feature preservation ability and classification robustness under different SNRs. The experimental results are shown in Figure 4.

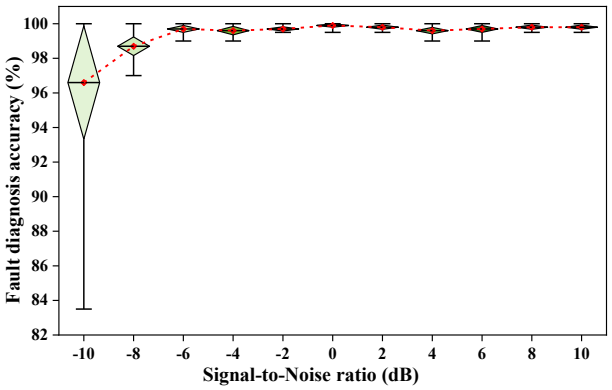

Figure 4. Diagnostic results under different signal-to-noise ratios

As illustrated in Figure 4, the accuracy of fault diagnosis gradually increases with the improvement of the SNR. When the SNR is low (e.g. -10 dB), the accuracy fluctuates widely, down to 83.5%, indicating that the noise has a large impact on the diagnostic results. When the SNR falls within the range of -8 dB to 0 dB, the diagnostic accuracy recovers with reduced fluctuation, demonstrating the model's enhanced noise immunity under moderate noise conditions. And the accuracy is almost stable at 100% at SNR higher than 0 dB, indicating that the proposed method is able to provide very stable and efficient fault diagnosis results at higher SNRs. Overall, the proposed method shows vulnerability to strong noise interference at low SNRs but maintains excellent diagnostic accuracy, exhibiting robust noise immunity. These findings offer solid support for deploying the proposed fault diagnosis method in practical industrial environments, ensuring diagnostic accuracy and stability even in the presence of substantial noise.

3.5 ALGORITHM COMPARATIVE ANALYSIS

To demonstrate the superiority of the proposed method, the experiment employs five hybrid algorithms for comparative validation, specifically including five different classifier architectures: (1) TF/FF-mRMR-CNN-Softmax; (2) TF/FF-mRMR-CNN-RF; (3)TF/FF-mRMR-CNN-DT; (4)TF/FF-mRMR-CNN-SVM and (5) its attention-enhanced version TF/FF-mRMR-CNN-Attention-SVM. All algorithms were evaluated for stability through five repeated trials. Table III summarizes the classification accuracy of each algorithm on the test set (mean ± standard deviation across trials) and the training time of a single trial.

TABLE III. COMPARATIVE REAULTS OF DIFFERENT ALGORITHMS

Method	First trial	Second trial	Third trial	Fourth trial	Fifth trial	Average accuracy (%)	Training time (s)
TF/FF-mRMR-CNN-Softmax	74.0%	65.0%	65.5%	67.5%	78.0%	70.0 ± 5.24	46.02
TF/FF-mRMR-CNN-RF	98.5%	100.0%	99.5%	98.5%	99.0%	99.10 ± 0.58	54.22
TF/FF-mRMR-CNN-DT	88.5%	95.0%	91.0%	92.0%	91.0%	91.50 ± 2.42	53.84
TF/FF-mRMR-CNN-SVM	**100.0%**	**100.0%**	**100.0%**	**100.0%**	**99.5%**	**99.90 ± 0.22**	**52.42**
TF/FF-mRMR-CNN-Attention-SVM	99.5%	100.0%	100.0%	99.0%	99.0%	99.65 ± 0.45	109.25

According to the experimental results in Table III, the performance of the five algorithms is significantly different. The TF/FF-mRMR-CNN-SVM performs the best with an average accuracy of 99.90% and very low volatility. The TF/FF-mRMR-CNN-RF achieves an accuracy of 99.10% but with a high standard deviation (0.58). The average accuracy of DT-based and Softmax-based methods respectively drops to 91.50% and 70.0%. The accuracy of TF/FF-mRMR-CNN-Attention-SVM, which introduces the attention mechanism, is comparable to that of TF/FF-mRMR-CNN-SVM, but the training time surges to 109.25 seconds. Overall, TF/FF-mRMR-CNN-SVM achieves the best balance between accuracy and efficiency and is the preferred method for this study.

4 CONCLUSIONS

This study addresses the challenge of industrial equipment fault diagnosis by proposing a novel diagnostic framework based on 1D-2D feature fusion and rigorously validates its effectiveness through systematic experimental evaluations. The main conclusions are summarized as follows: (1) The proposed method maintains high accuracy and robustness under varying loads and noisy environments, demonstrating excellent feature extraction capabilities. (2) The impact of sensor placement variations on the diagnostic accuracy is less than 2%, confirming that the proposed method is compatible with sensor deployment and provides a reliable solution for fault diagnosis in practical industrial applications.

REFERENCES

1. M. Hakim, A.A.B. Omran, A.N. Ahmed, M. Al-Waily, A. Abdellatif, A systematic review of rolling bearing fault diagnoses based on deep learning and transfer learning: Taxonomy, overview, application, open challenges, weaknesses and recommendations, Ain Shams Engineering Journal 14(4) (2023) 101945.
2. G. Nie, Z. Zhang, Z. Jiao, Y. Li, M. Shao, X. Dai, A novel intelligent bearing fault diagnosis method based on image enhancement and improved convolutional neural network, Measurement 242 (2025) 116148.
3. H. Yang, W.D. Li, K.X. Hu, Y.C. Liang, Y.Q. Lv, Deep ensemble learning with non-equivalent costs of fault severities for rolling bearing diagnostics, Journal of Manufacturing Systems 61 (2021) 249-264.
4. A.A. Soomro, M.B. Muhammad, A.A. Mokhtar, M.H. Md Saad, N. Lashari, M. Hussain, U. Sarwar, A.S. Palli, Insights into modern machine learning approaches for bearing fault classification: A systematic literature review, Results in Engineering 23 (2024) 102700.
5. B. Wang, W. Qiu, X. Hu, W. Wang, A rolling bearing fault diagnosis technique based on recurrence quantification analysis and Bayesian optimization SVM, Applied Soft Computing 156 (2024) 111506.
6. X. Dong, C. Zhang, H. Liu, D. Wang, Y. Chen, T. Wang, A new cross-domain bearing fault diagnosis method with few samples under different working conditions, Journal of Manufacturing Processes 135 (2025) 359-374.
7. X. Yan, M. Jia, Intelligent fault diagnosis of rotating machinery using improved multiscale dispersion entropy and mRMR feature selection, Knowledge-Based Systems 163 (2019) 450-471.
8. A. Ghasimi, S. Shamekhi, Enhanced EEG-based cognitive workload detection using RADWT and machine learning, Neuroscience 569 (2025) 231-244.
9. C. Cai, T. Xu, J. Ren, Y. Xue, Bearing Fault Diagnosis Based on the Markov Transition Field and SE-IShufflenetV2 Model, SDHM Structural Durability and Health Monitoring 19(1) (2024) 125-144.
10. C. Wu, S. Zheng, Fault Diagnosis Method of Rolling Bearing Based on MSCNN-LSTM, Computers, Materials and Continua 79(3) (2024) 4395-4411.